

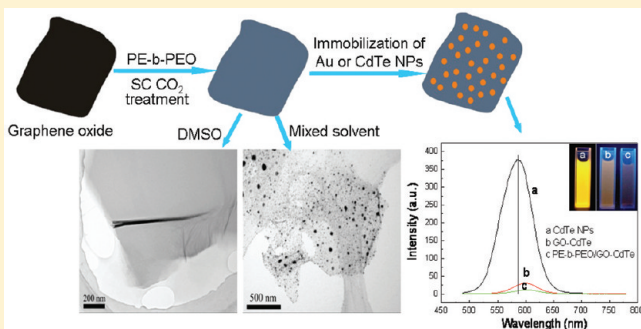
# Modification of Graphene Oxide with Amphiphilic Double-Crystalline Block Copolymer Polyethylene-b-poly(ethylene oxide) with Assistance of Supercritical CO<sub>2</sub> and Its Further Functionalization

Xiaoli Zheng, Qun Xu,\* Linghao He, Ning Yu, Shanshan Wang, Zhimin Chen, and JianWei Fu

College of Materials Science and Engineering, Zhengzhou University, Zhengzhou 450052, People's Republic of China

Supporting Information

**ABSTRACT:** Graphene oxide (GO) sheets were noncovalently modified with an amphiphilic double-crystalline block copolymer, polyethylene-b-poly(ethylene oxide) (PE-b-PEO) with assistance of supercritical CO<sub>2</sub> (SC CO<sub>2</sub>) in this work. The resulting PE-b-PEO/GO nanohybrids were characterized by transmission electron microscopy (TEM), wide-angle X-ray diffraction (WAXD), Fourier transform infrared spectroscopy (FTIR), and Raman spectra. Distinct morphologies of PE-b-PEO decorating on the surface of GO were obtained in different solvent systems and at different SC CO<sub>2</sub> pressures. We found that the solvent system and the SC CO<sub>2</sub> have significant influence on the crystallization, aggregation, or assembly behaviors of PE-b-PEO molecular chains on the GO sheets. The formation mechanism of the distinct nanohybrid structures is attributed to a relevant easy heteronucleation and the limited crystal growth of the block polymer on the surface of GO. The resulting modified GO sheets could find a broad spectrum of applications not only in producing graphene-based nanocomposites but also being used as a template to fabricate multifunctional structures due to the unique properties of PE-b-PEO. As a proof-of-concept, we further decorated the GO sheets with the as-prepared Au nanoparticles (Au NPs) and CdTe nanoparticles (CdTe NPs) with PE-b-PEO as the interlinker. Using the thiol-terminated PE-b-PEO as an interlinker, Au NPs can be densely assembled on the surface of GO via robust Au–S bonds. Furthermore, the photoluminescence quenching of CdTe NPs was more notable for PE-b-PEO/GO-CdTe hybrid compared to the GO-CdTe hybrid, suggesting that the electron transfer from the CdTe NPs to the GO sheets was enhanced with the PE-b-PEO interlinker. The availability of these affordable graphene-based multifunctional structures and their fundamental properties will open up new opportunities for nanoscience and nanotechnology and accelerate their applications.



## INTRODUCTION

Since its discovery, graphene has attracted considerable interest due to its extraordinary mechanical (Young's modulus  $\sim$ 1100 GPa),<sup>1</sup> electrical (charge carriers mobility up to  $200\,000\text{ cm}^2\text{ V}^{-1}\text{ s}^{-1}$ ),<sup>2</sup> and thermal properties (thermal conductivity  $\sim$ 5000 W m<sup>-1</sup> K<sup>-1</sup>).<sup>3</sup> However, it is difficult to produce and process on a large scale.<sup>4</sup> In addition, graphene contains rare surface functional moieties and very limited dispersibility in solvents, seriously limiting the exertion of its great potentials.<sup>5</sup> Graphene oxide (GO), produced by the oxidative treatment of graphite, is expected to realize the production of graphene in large quantities via reduction by chemical, thermal, or electrochemical techniques.<sup>6</sup> Furthermore, the incredibly large specific surface area, and the abundant oxygen-containing functional groups (e.g., hydroxyl, carboxyl, carbonyl, and epoxy groups) on GO afford GO sheets great promise for many more applications.<sup>7–12</sup> For instance, the GO nanosheets provide an ideal substrate for enzyme immobilization by interactions between enzyme molecules and the functional groups of GO.<sup>9</sup> The intrinsic oxygen-containing functional groups have also been used as reactive sites for deposition of metal or metal oxide nanoparticles,

which open up widespread applications in fields such as catalysts, supercapacitors, biodetection, biosensors and so on.<sup>13–18</sup> Goncalves et al. showed that the nucleation and growth mechanism of gold nanoparticles depends on the degree of oxygen functionalization at the graphene surface sheets, no gold nanoparticles are obtained on totally reduced graphene surfaces.<sup>13</sup> What's more, Ramanathan et al. reported that the oxygen and hydroxyl functional groups on the functionalized graphene are well suited to form composites with polar polymers such as poly(methyl methacrylate) (PMMA), poly(acrylonitrile) (PAN), and poly(acrylic acid) (PAA), giving rise to intimate nanosheet–polymer interactions and a percolated interphase, which are essential to mechanical and thermal enhancement.<sup>19</sup>

Recently, modification of GO has aroused great interest because GO sheets can only be dispersed in many polar solvents such as water and dimethylformamide (DMF), and reduction

**Received:** February 23, 2011

**Revised:** April 4, 2011

**Published:** April 26, 2011

of aqueous-dispersed GO would lead to their irreversible agglomeration.<sup>20</sup> Given that GO consists of plentiful oxygen-containing functional groups and carbon atoms linked by  $sp^2$  bonds as the carbon nanotubes (CNTs), various methods for functionalization of GO have also been employed.<sup>5,20–29</sup> Among these methods, polymer-modified GO is particularly attractive because it endows GO with great potential for applications in biomedical and nanocomposite fields.<sup>20,24–29</sup> For example, GO nanosheets modified with polyethylene glycol have been employed as aqueous compatible carriers for water-insoluble drug delivery.<sup>24</sup> In another parallel research field, polymers, especially the block polymers, have been used to modify carbon nanotubes (CNTs).<sup>30–33</sup> Block polymers enhance the dispersibility and stability of CNTs in a wider range of organic solvents and host polymer matrices than homopolymers.<sup>30</sup> More attractively, compared to the homopolymers, block polymers are more susceptible to the surrounding environment in solution, such as solvent composition, temperature, pH, copolymer concentration, and the additives.<sup>34–40</sup> With the change of any one of these parameters, block copolymers are able to present microphase separation and self-assemble to form a range of different morphologies. These particular microstructures have many potential applications in various fields, such as cosmetics, drug delivery, electronics, pollution control, and advanced materials formation and separation.<sup>41–43</sup> Therefore, it is intriguing to investigate the decorating morphologies of block copolymer on GO sheets, and the block copolymer modification may impart significant advantages to the resulting GO sheets such as for preparing GO-based nanocomposites, serving as a catalyst support, directing nanoparticle assembly or acting as biosensor. However, few studies about the decorating morphology of block polymers on GO have been reported to date.<sup>44</sup>

In our previous study, we found that supercritical fluid can serve as an effective external field to help construct specific molecular structures on CNTs.<sup>45</sup> By virtue of the antisolvent effect of supercritical CO<sub>2</sub> (SC CO<sub>2</sub>), nanohybrid shish-kebabs of PE decorated CNTs can not only be achieved but also their sizes and periodicity can be controlled directly by various conditions such as pressure, temperature, solvent, and so on. So it triggers our interest to investigate the decorated morphologies of block copolymer on GO sheets with the assistance of SC CO<sub>2</sub>. More recently, double crystalline block copolymers have begun to receive attention, because the crystalline blocks can increase the complexity of the system, which may lead to unexpected novel properties.<sup>46–50</sup> Polyethylene-b-poly(ethylene oxide) (PE-b-PEO), a typical amphiphilic double-crystalline block copolymer, presents unique aggregation morphology and the confined crystallization in the micro- and/or nanoscale self-assembled structure.<sup>51–55</sup> Additionally, the PEO segment is a biocompatible polymer and has very important application in biotechnologies and pharmaceuticals since it resists protein adsorption and cell adhesion.<sup>56,57</sup> Li et al. showed that PE-b-PEO can be periodically decorated along single-walled carbon nanotubes, leading to amphiphilic and alternating patterns.<sup>58</sup> In this work, a relatively low molecular weight of double-crystalline block copolymer PE-b-PEO (with 29 and 20 repeating units in the PE and PEO blocks, respectively) was used to decorate GO with assistance of SC CO<sub>2</sub>. We investigated the influence of solvent composition and SC CO<sub>2</sub> pressure on the morphologies of PE-b-PEO on GO. And the formation mechanism of the corresponding decorated morphology was discussed in this work. The resulting modified GO sheets could find a broad spectrum of

applications not only in producing graphene-based nanocomposites but also in acting as a template to fabricate multifunctional structures due to the unique properties of PE-b-PEO. As an example, as-prepared Au nanoparticles (Au NPs) and CdTe nanoparticles (CdTe NPs) were immobilized on the modified GO sheets successfully by using PE-b-PEO as an interlinker. These nanohybrid structures may build a favorable foundation for fabricating graphene-based functional nanodevices.

## ■ EXPERIMENTAL SECTION

**Materials.** Natural graphite powder ( $\leq 30\ \mu\text{m}$ , with purity >99.85 wt %) was purchased from Sinopharm Chemical Reagent Co., Ltd., People's Republic of China. GO was prepared with natural graphite powder through a modified Hummers method.<sup>59,60</sup> Raw low molecular weight PE-b-PEO (number-average molecular weight 1400 g/mol, 50 wt % PEO), and HAuCl<sub>4</sub> were purchased from Aldrich and used as received. Thioglycolic acid and mercaptoacrylic acid were purchased from Acros Organics. Sodium borohydride was purchased from Guangdong Guanghua Chemical Factory Co., Ltd. Other chemicals, dimethyl sulfoxide (DMSO), *p*-xylene, sulphuric acid (98%), isopropyl ether, dichloromethane, toluene, cadmium chloride, tellurium power, trisodium citrate, HCl, and NaOH were all purchased from Sinopharm Chemical Reagent Co., Ltd. (People's Republic of China) and used as received. Aqueous solutions were prepared with double-distilled water from a Millipore system.

**Exfoliation of GO and Modification by PE-b-PEO.** A 0.1-mg portion of GO was dispersed in 2 g of DMSO or 1.5 g of DMSO/0.5 g of *p*-xylene, and ultrasonicated for 30 min to obtain homogeneous GO brown solution. Meanwhile, 1.5 mg of PE-b-PEO was dissolved in 3 g of DMSO or 3 g of *p*-xylene at a suitable temperature before being added into GO solution under ultrasonication. The mixture was then quickly transferred into the SC CO<sub>2</sub> apparatus to reach the determined conditions of temperature and pressure. The reaction time in the condition of SC CO<sub>2</sub> was controlled to be 3 h and then the system was slowly depressurized and the sample was collected. A comparison study was also made by treating the pure polymer in the same SC CO<sub>2</sub> condition as the corresponding nanohybrid prepared.

**Synthesis of Thiol-Terminated PE-b-PEO.** Thiol-terminated PE-b-PEO was synthesized by reacting the hydroxyl terminated PE-b-PEO with thioglycolic acid as described by Li et al. (see the Supporting Information for details about the preparation process).<sup>58</sup> The same experimental procedure was performed to modify GO with thiol-terminated PE-b-PEO using DMSO as the solvent.

**Immobilization of Au NPs and CdTe NPs on Modified GO Sheets.** Au NPs and CdTe NPs were synthesized according to the procedure described by Fang et al.<sup>61</sup> and Zhang et al.,<sup>62</sup> respectively (see the Supporting Information for details of the preparation process). The as-prepared thiol-terminated PE-b-PEO/GO nanohybrids were used to immobilize Au NPs. Two assembly methods were used and the details were described as follows. The first method (incubation method): the as-prepared thiol-terminated PE-b-PEO/GO DMSO solution was drop cast on a TEM micro grid and dried at ambient temperature for 5 min. Then the grid was incubated with the as-prepared Au NPs aqueous solution for 2 h. The grid was rinsed with double-distilled water two times and dried at ambient temperature before TEM characterization. The second method (mixed method): a 0.7 mL portion of thiol-terminated PE-b-PEO/GO

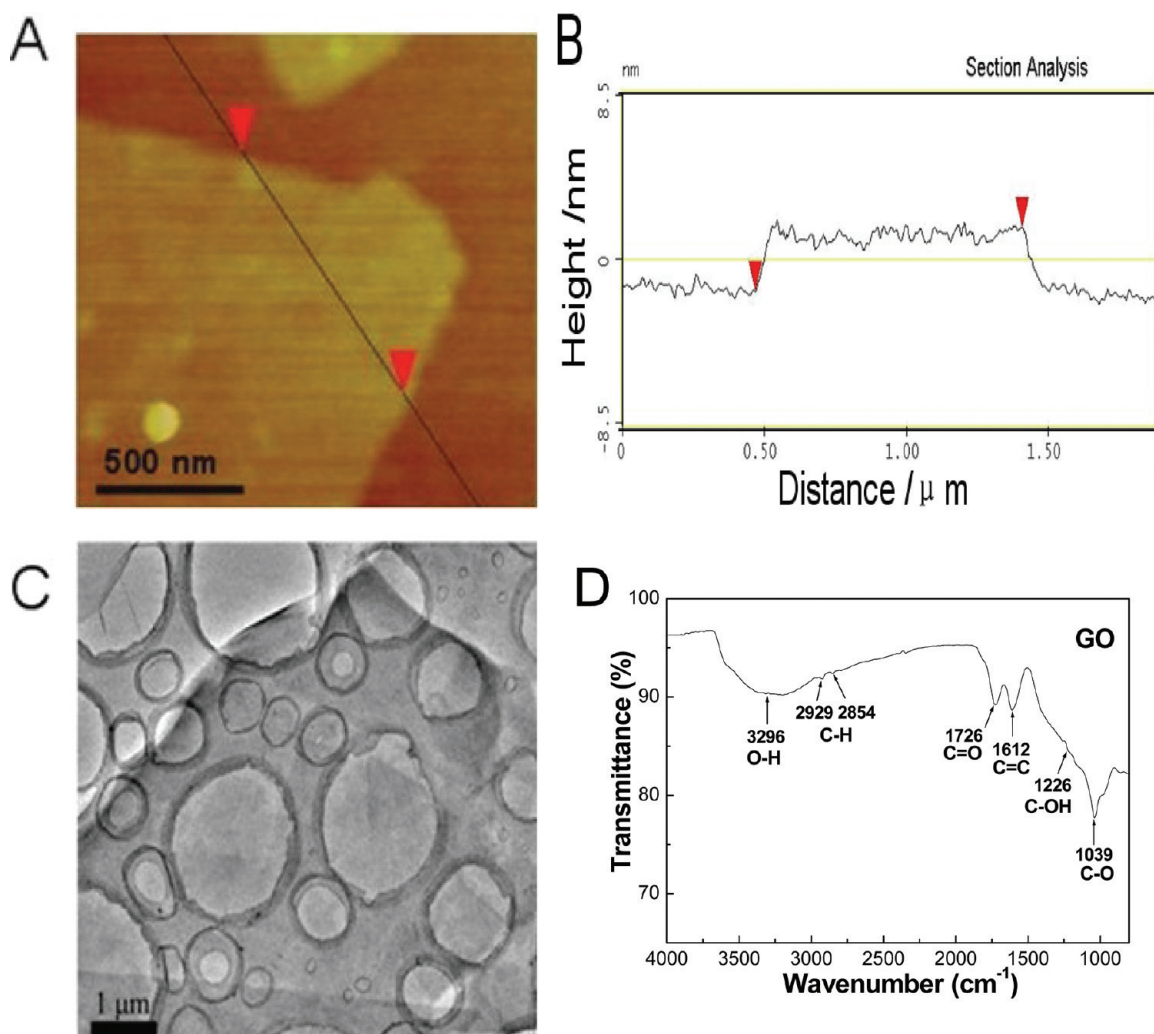


**Figure 1.** (A) Tapping mode AFM image of graphene oxide (GO) on a mica surface, (B) height profile of the AFM image, (C) TEM image of the GO, and (D) FTIR spectrum of GO.

DMSO solution was added into 4 mL of Au NPs solution under stirring. Then the mixture was sonicated for 2 min before standing overnight. Finally, the precipitate was collected by centrifugation and washed by double-distilled water for two times. The as-prepared Au NPs/thiol-terminated PE-b-PEO/GO hybrid was redispersed in 1 mL of water. For attachment of CdTe NPs, the PE-b-PEO/GO nanohybrid was used directly: 2 mL of PE-b-PEO/GO DMSO solution was added into 2 mL of CdTe NPs solution under stirring. Then the mixture was sonicated for 2 min. The resulting solution was directly used to conduct the TEM characterization. The solution was isothermally ultrasonicated for 10 min to remove the free CdTe NPs and then a drop of the dispersion was deposited on a TEM carbon-covered grid.

**Characterization.** A Digital Instruments MultiMode scanning probe microscope with a Nanoscope IIIA controller in tapping mode was used for the AFM measurements. Transmission electron microscopy (TEM) (FEI Tecnai G2 20) experiments were conducted with an accelerating voltage of 120 kV. FT-IR spectra were recorded using a BRUKER TENSOR27 instrument with a resolution of  $2\text{ cm}^{-1}$ . KBr was used to prepare sample pellets. Wide angle X-ray diffraction (WAXD) was carried out using a Y-2000 X-ray Diffractometer with CuK $\alpha$  radiation

( $\lambda = 0.15406\text{ nm}$ ) operating at 40 kV and 40 mA. Raman spectra were obtained at 514.5 nm laser excitation on a Renishaw Microscope System RM2000 at room temperature. The laser power density was kept less than 3 mW with a resolution of  $1.5\text{--}2.0\text{ cm}^{-1}$  over the spectral window. Spectra were collected at various locations on each sample studied to determine reproducibility. Ultraviolet-visible (UV-vis) absorption spectral measurements were carried out with a Shimadzu UV-240/PC spectrophotometer. Photoluminescence (PL) spectra were measured on a Deinburgh FL/FS TCSPC 920 spectrofluorophotometer.

## RESULTS AND DISCUSSION

**Characterization of GO.** The as-prepared graphite oxide can be ultrasonically exfoliated to graphene oxide (GO), which readily forms a stable colloidal suspension in DMSO. The morphology of the GO was obtained with an atomic force microscope (AFM) in a tapping mode (Figure 1A). The AFM micrograph of GO shows that the thickness of the resulting GO sheets is  $\sim 3.3\text{ nm}$  (Figure 1B), suggesting that the GO film consists of two or three atomic layers thickness structure feature.<sup>13</sup> The thin nanoplate motif of the GO sheet was also confirmed by TEM (Figure 1C). Two or three layers of translucent GO sheets are overlapped

together with rolled edges. The presence of the functional groups is confirmed by the FT-IR spectrum of GO (Figure 1D), which displays a consistency with that reported by Wu et al.<sup>25</sup> The most prominent feature in the spectrum is the adsorption band corresponding to the O—H stretching vibrations at 3600–3200 cm<sup>-1</sup>. The peaks at 2929 and 2854 cm<sup>-1</sup> correspond to the presence

**Table 1. Solubility Parameters of Different Polymers and Different Solvents**

samples	solubility parameter (cal/cm <sup>3</sup> ) <sup>1/2</sup>
PE	8.0
PEO	10.2
p-xylene	8.75
DMSO <sub>5</sub> <sup>a</sup>	13.4
DMSO <sub>1.5</sub> <sup>a</sup> /p-xylene <sub>3.5</sub> <sup>a</sup>	10

<sup>a</sup>The weight of corresponding solvent used in this work. When using the mixed solvent, the solubility parameter of the mixed solvent ( $\delta_{\text{mixed}}$ ) can be calculated by the following equation:  $\delta_{\text{mixed}} = \Phi_1 \delta_1 + \Phi_2 \delta_2$ , Here  $\Phi_1$  and  $\Phi_2$  are the volume fractions of two pure solvents, respectively.  $\delta_1$  and  $\delta_2$  are the solvent parameters of two pure solvents.<sup>64</sup>

of a C—H bond. The absorption peak at 1726 cm<sup>-1</sup> is due to —C=O stretching, whereas the band at 1612 cm<sup>-1</sup> is attributed to —C=C— stretching as part of the ring breathing mode in the GO skeleton. The absorption peaks at 1226 and 1039 cm<sup>-1</sup> are attributed to the stretching vibration of the C—OH of phenols and C—O groups, respectively.<sup>20</sup> These abundant, oxygen-containing groups are expected to form robust interactions with other groups.

**Decorated Morphologies of PE-b-PEO on the Surface of GO in Different Solvent Systems.** Note that solvent selectivity is critical to solution crystallization of crystalline block copolymer.<sup>63</sup> In this work, we used two different solvent systems: pure DMSO and mixed solvent DMSO/p-xylene to study the decorated morphology of PE-b-PEO on the surface of GO. The solubility parameters of polymers and the two solvent systems are provided in Table 1.<sup>64</sup>

Figure 2 shows the TEM images and electron diffraction pattern of PE-b-PEO/GO nanohybrids prepared in different solvents with the assistance of SC CO<sub>2</sub>. In Figure 2A,B, the GO sheets are decorated with thick block copolymer PE-b-PEO coatings with small black dots at their edge. The average diameters

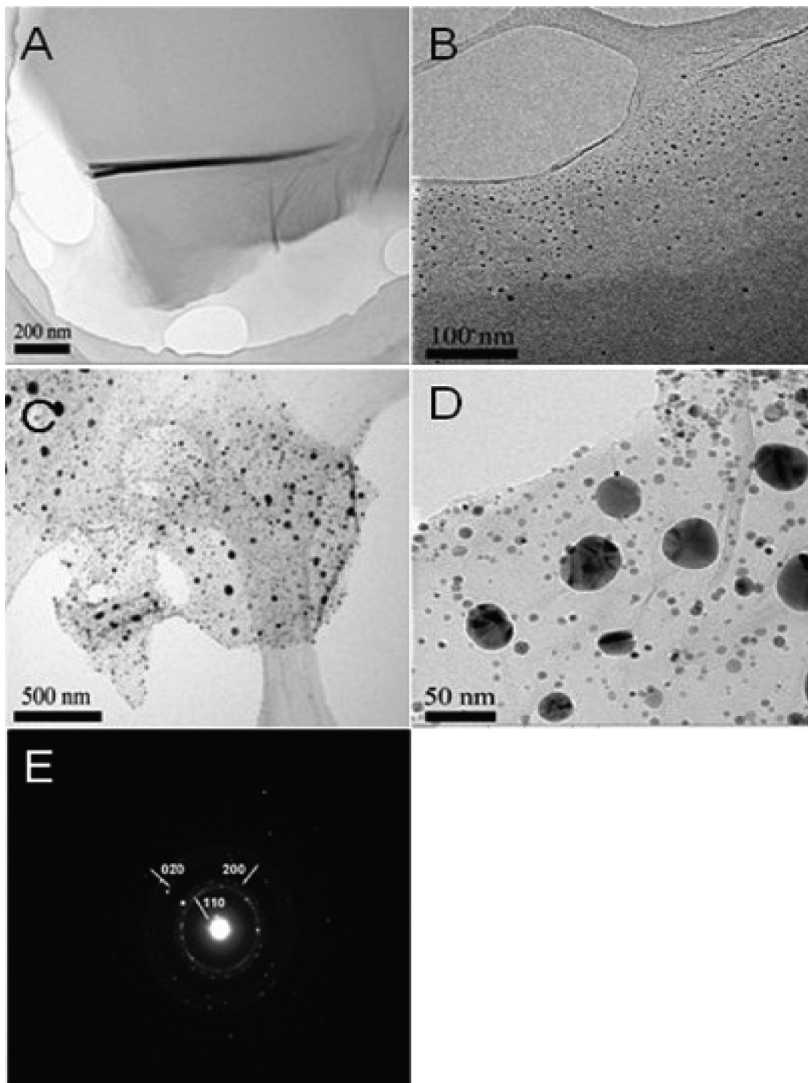


**Figure 2.** TEM images and electron diffraction pattern of PE-b-PEO/GO nanohybrids produced in the same SC CO<sub>2</sub> condition (90 °C, 13 MPa for 3 h) and PE-b-PEO concentration (0.03 wt %) and GO concentration (0.002 wt %), but in different solvents: (A, B) DMSO; (C, D, E) the mixed solvent.

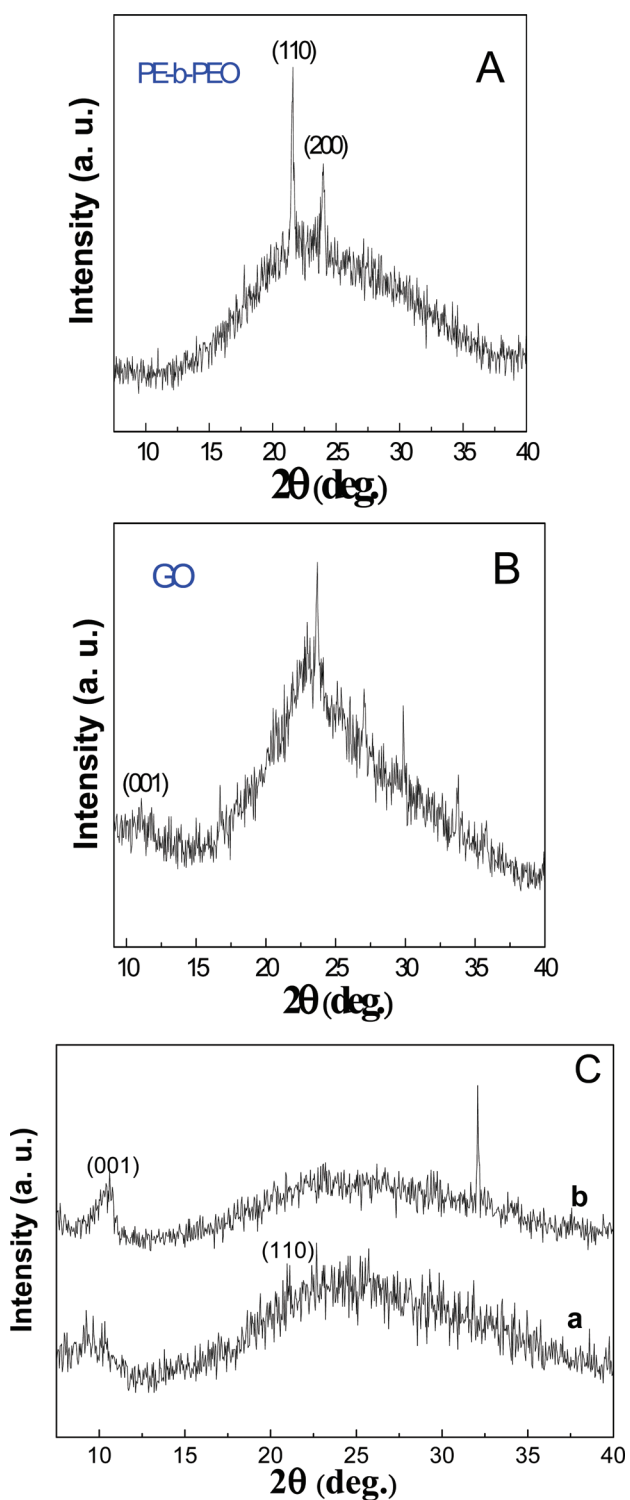


**Figure 3.** Wide-angle X-ray diffraction patterns of (A) pure PE-b-PEO, (B) GO, and (C) PE-b-PEO/GO nanohybrids produced in different solvents: (a) the mixed solvent, (b) DMSO, treated in SC CO<sub>2</sub> at 90 °C and 13 MPa for 3 h, and PE-b-PEO concentration (0.03 wt %) and GO concentration (0.002 wt %). The pure PE-b-PEO was treated in the same SC CO<sub>2</sub> condition as the nanohybrid of (a).

of the dots are in the range of 3–6 nm, which resembles the result of poly(vinyl alcohol) (PVA) decorated on CNTs.<sup>65</sup> However, when the mixed solvent is used, the surface of GO is fully decorated

with varying sizes of dots (4–40 nm) (Figure 2C,D). It can be clearly seen that some large dots are in the form of crystals. On the corresponding electron diffraction pattern (Figure 2 E), the sharp reflection rings confirm that the nanodots exhibit a high degree of crystallinity. In addition, the characteristic (110), (200), and (020) diffractions of the PE can be observed, indicating that the nanocrystals consist of PE crystals. Given that the crystallization temperature ( $T_c$ ) is relatively high (90 °C), PEO is in the form of amorphous state on the surface of GO.<sup>52</sup> The adsorption of block copolymers onto various solid substrates has been extensively studied for the reason that it provides a useful way to obtain different structures on the solid surfaces.<sup>66–68</sup> Depending on the block copolymer/GO/solvent interaction parameters, two scenarios are possible: (i) the block copolymer form micelles first and then adsorb on the surface of GO sheets; (ii) the block copolymer chains adsorb onto the GO sheets and then aggregate together. Note that the concentration of the solution of the resultant PE-b-PEO ( $C \approx 0.3$  mg/mL) is quite low, at which PE-b-PEO individual chains could not aggregate in the solution. Additionally, as shown in Table 1, DMSO is more selective for PEO, so micelles would form more easily in DMSO than in the mixed solvent. Whereas the contrary results shown in Figure 2 clearly indicate that the scenario (ii) is the dominant physical process. It indicates that the solvent plays an important role in the morphology of PE-b-PEO on GO. The detailed formation mechanism of these distinct patterning behaviors of PE-b-PEO on GO would be discussed in the following section.

To obtain a further understanding of the crystallization behavior of PE-b-PEO on the surface of GO, WAXD experiment was carried out. Figure 3 shows the XRD patterns of pure PE-b-PEO (A), GO (B), and PE-b-PEO/GO nanohybrids produced in different solvents (C). For pure block copolymer PE-b-PEO, the crystalline peaks appear at  $2\theta = 21.6^\circ$  and  $24^\circ$ , corresponding to (110) and (200) reflections from the orthorhombic unit cell of PE.<sup>69</sup> The XRD does not show any diffraction peak of PEO,<sup>70</sup> indicating that the crystallization behavior of PEO has been heavily disturbed due to the relatively high crystallization temperature ( $T_c$ ). For GO, the diffractions peaks near 11° and 24° can be attributed to graphite-like structure (001) and (002), respectively.<sup>71,72</sup> The X-ray data of PE-b-PEO/GO nanohybrids produced in different solvents are presented in Figure 3C. For PE-b-PEO/GO nanohybrids, the (001) diffraction peak of GO shifts to lower angle. The corresponding interlayer spacings are (a) 9.6 Å, (b) 8.3 Å, which are larger than that of the original GO (8.0 Å), indicating that GO is successfully modified by PE-b-PEO.<sup>73</sup> From Figure 3C, we can find that the crystallinity of PE-b-PEO is severely interrupted in the nanohybrids, especially in the case (b) that PE-b-PEO presents an amorphous state, which is consistent with the results shown in Figure 2.

Webber et al. reported that the structure of block copolymer was influenced by the interactions between the polymer chains and the substrate.<sup>74</sup> In this work, the interfacial interaction between the block copolymer molecules and GO was investigated by FT-IR spectroscopy and Raman spectroscopy. The FTIR spectra for pure PE-b-PEO and PE-b-PEO/GO nanohybrids produced in different solvents are shown in Figure 4. Table 2 summarizes the frequencies of the important absorption bands and the associate assignments. Obviously, the characteristic spectra of PE-b-PEO are also present in the nanohybrids. In the pure PE-b-PEO, five absorption bands observed at 2917, 2850, 1473, 1462, and 719 cm<sup>-1</sup> are related to PE chain segmental parts. The rest absorption bands with an arrow are from PEO segments (Figure 4A).<sup>75</sup>

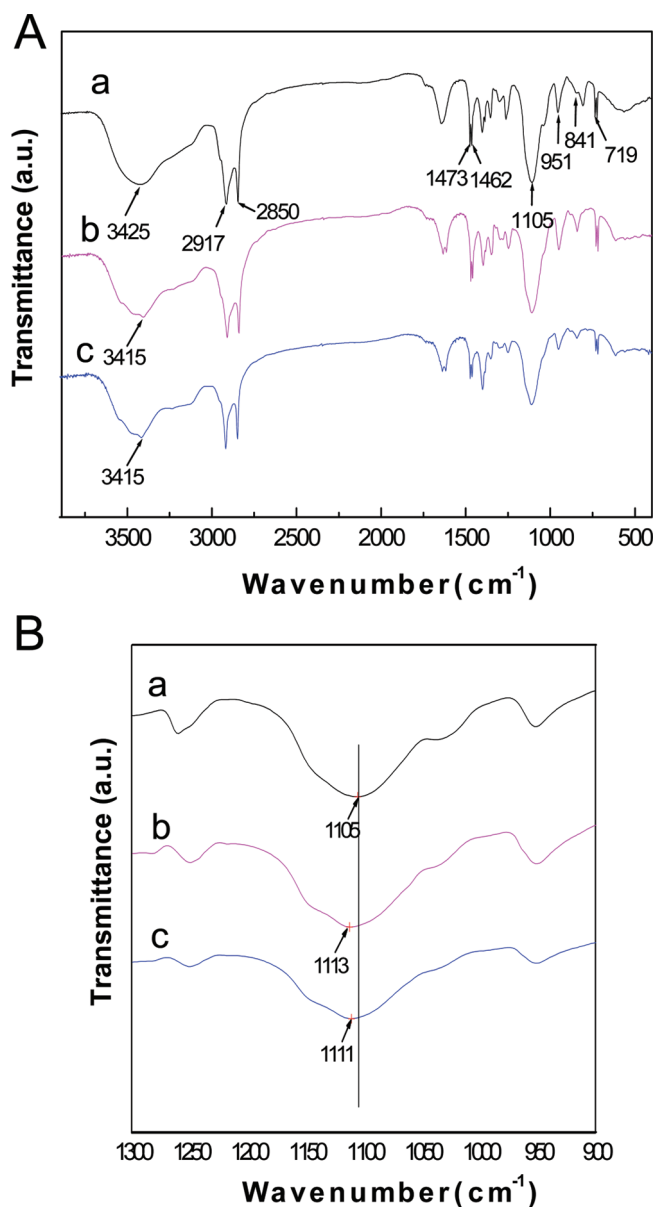


**Figure 4.** FTIR spectra (A) from 3900 to 400 cm<sup>-1</sup> and (B) from 1300 to 900 cm<sup>-1</sup> of pure PE-b-PEO (a) and PE-b-PEO/GO nanohybrids produced in different solvents: (b) the mixed solvent, (c) DMSO, treated in SC CO<sub>2</sub> at 90 °C and 13 MPa for 3 h, and PE-b-PEO concentration (0.03 wt %) and GO concentration (0.002 wt %). The pure PE-b-PEO was treated in the same SC CO<sub>2</sub> condition as the nanohybrid of (b).

Compared with the IR spectrum of pure polymer, the spectra related to PE segments in the PE-b-PEO/GO nanohybrids show a minute shift, which is similar to the results of the PE/SWNT nanohybrid.<sup>76</sup> The results indicate that there exist noncovalent and nonspecific CH-π interactions between PE chains and GO sheets.<sup>77</sup> This favorable physical interaction between GO sheets and PE segments may make PE-b-PEO easily adsorb onto the GO surface and lead to a remarkable nucleation effect. Whereas for the spectra assigned to the PEO segment in the nanohybrids, which show significant displacements in certain regions. For pure PE-b-PEO, the peak at around 3425 cm<sup>-1</sup> is assigned to stretching vibration of —OH in the terminal chain of PEO. The peak becomes

**Table 2.** FTIR Absorption Bands and Their Assignments of PE-b-PEO (a) and PE-b-PEO/GO Nanohybrids Produced in Different Solvents (b, c) (3900–400 cm<sup>-1</sup>)<sup>a</sup>

assignment	frequency (cm <sup>-1</sup> )		
	a	b	c
PE			
$\nu$ (CH <sub>2</sub> ) <sub>a/s</sub>	2917/2850	2920/2848	2918/2848
$\delta$ (CH <sub>2</sub> )	1473/1462	1473/1462	1473/1462
$r$ (CH <sub>2</sub> )	719	721	720
PEO			
$\nu$ (OH)	3425	3415	3415
$\nu$ (COC)	1105	1113	1111
$r$ (CH <sub>2</sub> ) <sub>a/s</sub>	951/841	951/843	953/843

<sup>a</sup> Mode assignments:  $\nu$  (stretching);  $\delta$  (bending);  $r$  (rocking). The subscripts a and s denote the asymmetric and symmetric motions with respect to the twofold axis perpendicular to the helix axis and passing through the O atom or through the C—C bond.

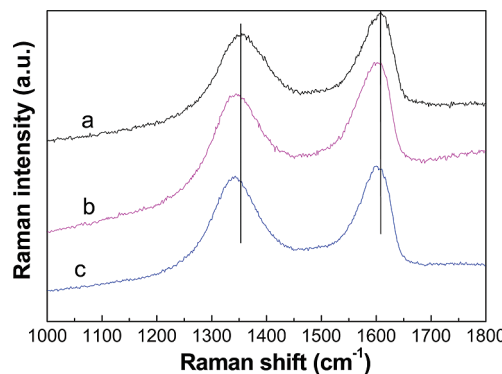


**Figure 5.** Raman spectra of GO (a) and PE-b-PEO/GO nanohybrids produced in different solvents: (b) the mixed solvent, (c) DMSO, treated in SC CO<sub>2</sub> at 90 °C and 13 MPa for 3 h, and PE-b-PEO concentration (0.03 wt %) and GO concentration (0.002 wt %). The GO was treated in the same SC CO<sub>2</sub> condition as the nanohybrid of (b).

sharpened and shifts significantly in PE-b-PEO/GO nanohybrids (Figure 4A). In the region of 1300–900 cm<sup>-1</sup> shown in Figure 4B, it is highlighted that the peak near 1105 cm<sup>-1</sup> in PE-b-PEO is for asymmetric stretching vibration of the C—O—C group.<sup>78</sup> Whereas, the C—O—C stretching vibrations of the nanohybrids shift to higher frequency compared to that of pure PE-b-PEO. These results indicate that there exist significant interactions between PEO segments and the GO sheets. Considering the great number of oxygen-containing functional groups (e.g., hydroxyl, carboxyl, and epoxy groups) on the surface of GO sheets, and terminal hydroxyl groups and electron rich ether oxygen in the PEO chain segmental parts, significant physical interactions such as hydrogen bond may form between GO and PEO segments.

Further evidence for interconnectivity of PE-b-PEO with GO was obtained from Raman spectroscopy. Figure 5 shows the high frequency Raman spectra for GO and PE-b-PEO/GO nanohybrids produced in different solvents. Raman spectra of GO sheets display two broad picks at 1355 and 1609 cm<sup>-1</sup>, which represent the D-band (C—C, the vibrations of sp<sup>3</sup> carbon atoms of defects

and disorder) and G-band ( $C=C$ , the vibration of  $sp^2$  carbon atoms in a graphitic 2D hexagonal lattice), respectively.<sup>72</sup> In general, the degree of graphitization is an indicator of the graphene sheets' disorder level and is characterized by the intensity ratio of the D and G bands ( $R = I_D/I_G$ ). The D- and G- bands and  $I_D/I_G$  intensity ratios of GO and PE-b-PEO/GO nanohybrids produced in different solvents are listed in Table 3. The high intensity ratio of GO ( $I_D/I_G = 1.37$ ) indicate that the graphitic 2D hexagonal lattice has been severely disturbed. After being decorated with PE-b-PEO, the  $I_D/I_G$  intensity ratios of PE-b-PEO/GO (shown in Table 3) are similar to that of pristine GO, indicating that the electronic structure of GO is preserved well by the noncovalent functionalization of PE-b-PEO. In addition, we observed that the peak positions of the D-band and G-band in PE-b-PEO/GO nanohybrids show significant and comparable down-shift compared with the spectrum of GO. Rao et al.<sup>79</sup> and Voggu et al.<sup>80</sup> pointed out that the down-shift of the G bands is a consequence of *n*-type doping. Chatterjee et al. also reported that favorable interactions between the polymer and the SWNTs can decrease the G-band frequency.<sup>81</sup> It indicates that there exists favorable interaction between *n*-orbitals of PEO ether oxygen and the  $\pi$ -system of GO sheets. From the results of FTIR and Raman, we find that there exist significant interactions between block copolymer chains and GO sheets, which can also have significant effect on the morphology of PE-b-PEO on GO.

**Table 3. Raman D- and G- Bands and  $I_D/I_G$  Intensity Ratios of GO and PE-b-PEO/GO Nanohybrids Produced in Different Solvents<sup>a</sup>**

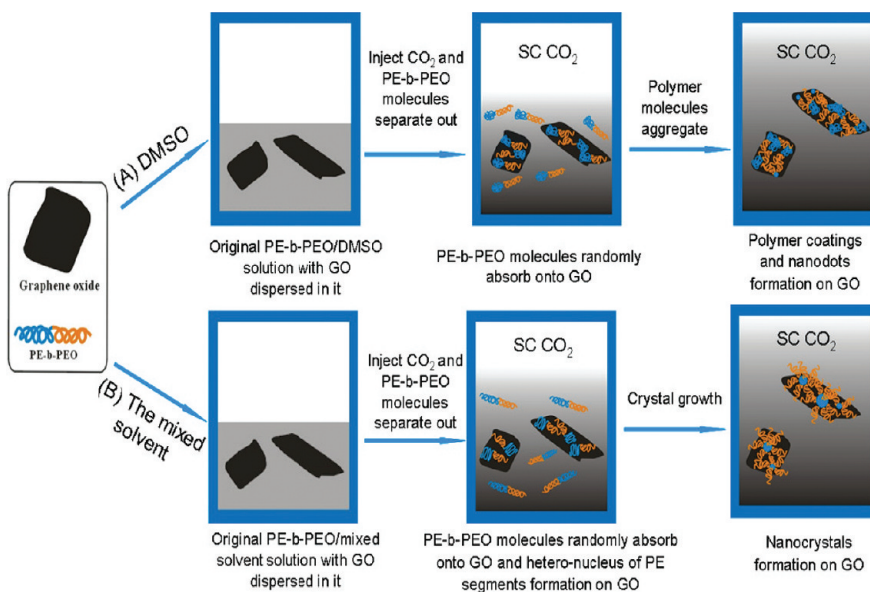
samples	D-band ( $\text{cm}^{-1}$ )	G-band ( $\text{cm}^{-1}$ )	$I_D/I_G$
a	1355	1609	1.37
b	1343	1601	1.40
c	1343	1600	1.48

<sup>a</sup> The  $I_D/I_G$  intensity ratios were calculated by the ratios of peak areas of D- and G- bands. The peak areas of D- and G- bands were obtained by baseline corrections and being fitted with Lorentzian function.

**Formation Mechanism of the Different Morphologies of PE-b-PEO on GO in Different Solvent Systems.** From the above discussion, we find that the solvent system and the interactions between PE-b-PEO chains and 2D GO nanosheets have significant influence on morphologies of PE-b-PEO on GO. The formation mechanism of the distinct nanohybrid structures is attributed to a relevant easy heteronucleation and the limited crystal growth of the polymer on the surface of GO. The mechanism is suggested as follows. With the injection of SC  $\text{CO}_2$ , the volume of the original PE-b-PEO solution with exfoliated GO sheets is expanded and its solvent power on polymer is reduced, which can lead to the PE-b-PEO molecules separating out of the supersaturated solution. During the separation of the molecular chains, the block copolymer PE-b-PEO molecules randomly adsorb onto the GO surface due to the favorable interactions between the polymer chains and GO. Given that GO consists of plentiful oxygen-containing functional groups and carbon atoms linked by  $sp^2$  bonds as those of the carbon nanotubes (CNTs), the PE segments are easy to heterogeneously nucleate on the surface of GO. While the PEO segments form robust interactions with oxygen-containing functional groups on GO, which restricts the movement of molecular chains and leads to block copolymer phase separation.

Compared with the mixed solvent, DMSO is more selective for PEO (shown in Table 1), so the PE segment become less loosely packed in the system of DMSO. When DMSO is used as the solvent, the PE chains curl up due to the selectivity of DMSO, which impedes the effective heteronucleation of PE chains on the surface of GO. So finally the PE-b-PEO chains have to form random coatings with a few little nanodots aggregated by several molecular chains on the surface of GO. When using the mixed solvent, the PE segments are relatively loose and conduct heterogeneous nucleation on the GO sheets everywhere. During the separation of the molecular chains, the local concentration increase near the surface of GO and more PE chains crystallize on the prenuclei. Taking into account the confinement of connected PEO chains and the considerable two-dimentional flat area of the GO sheets, block copolymer can only form aggregated spherical crystals on GO due to the mismatch between the

**Scheme 1. Schematic Representations of the Hypothetical Mechanism of PE-b-PEO Nanohybrid Superstructures Formation Process with the Assistance of SC  $\text{CO}_2$  in Different Solvents: (A) DMSO, (B) the Mixed Solvent**



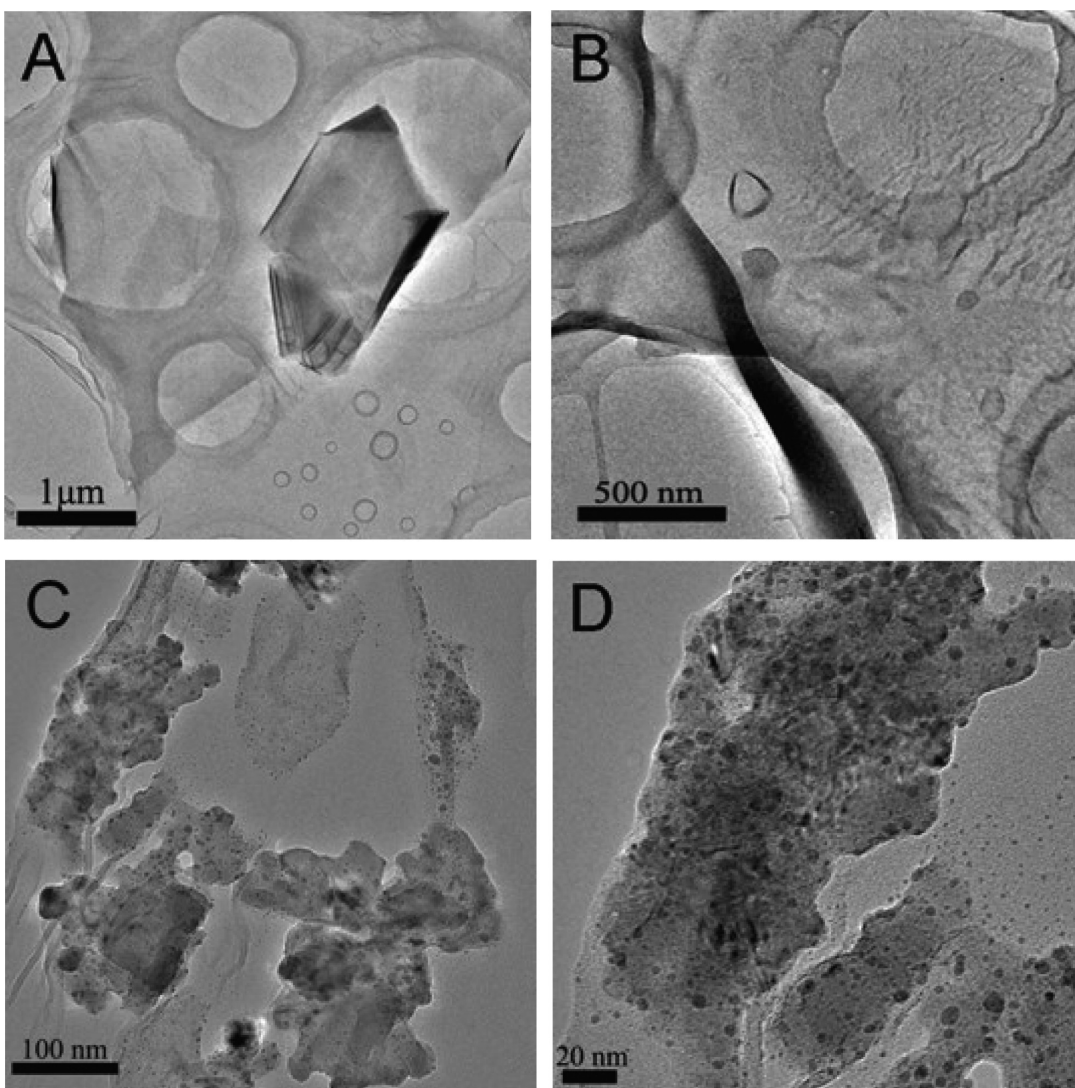


**Figure 6.** TEM images of PE-b-PEO/GO nanohybrids produced in the same SC CO<sub>2</sub> condition (90 °C, 13 MPa for 3 h) and PE-b-PEO concentration (0.03 wt %) and GO concentration (0.002 wt %) in the mixed solvent, but at different pressures: (A, B) 11 MPa; (C, D) 15 MPa.

dimensions of GO and the aggregates.<sup>82</sup> The formation of the large sizes of crystals may result from the cumulative crystallization of a large number of PE-b-PEO chains. The detailed formation procedure is illustrated in Scheme 1.

**Effect of SC CO<sub>2</sub> Pressure on the Morphologies of PE-b-PEO on GO.** For SC CO<sub>2</sub>, experimental pressure has an important effect on the solvent power. Therefore, we tune the experimental pressure of SC CO<sub>2</sub> from 13 to 11 and 15 MPa, respectively, and study the effect of SC CO<sub>2</sub> pressure on the decorated morphology of PE-b-PEO. According to the literature,<sup>83</sup> at the same temperature of 90 °C, the solvent density of CO<sub>2</sub> increases with pressure. The antisolvent effect of SC CO<sub>2</sub> is determined by the solvent density of CO<sub>2</sub>. The obtained results are shown in Figure 6. We find that when the pressure reduces to 11 MPa, only a continuous monolayer with few polymer dimples forms on the GO surface (Figure 6A,B). It indicates that when the pressure is low, the antisolvent effect of SC CO<sub>2</sub> is weak, and the amount of the PE-b-PEO chains separation is so low that few PE-b-PEO chains absorb onto the GO sheets and hardly grow into crystals. Whereas, if the pressure is excessively high (15 MPa), both the amount and speed of the polymer chain separation is greatly

increased so that the block copolymer molecules accumulate and form large irregular aggregates on the surface of GO. Then with the decrease of the amount of block copolymer separating from the solution, some small spherical crystals of PE-b-PEO are formed both on the GO sheets and the large aggregates due to the heterogeneous crystallization of the later adsorbed PE-b-PEO chains (Figure 6C,D). Therefore, there exists an optimum SC CO<sub>2</sub> pressure at which the well-defined spherical crystals are formed on the surface of GO, which is 13 MPa. A control experiment was conducted by decorating GO with PE-b-PEO in mixed solvent without the treatment of SC CO<sub>2</sub> (Figure S1 of the Supporting Information (SI)). No nanocrystals are observed and the corresponding electron diffraction pattern (Figure S1B of the (SI)) further confirms the amorphous state of PE-b-PEO on the surface of GO, indicating that the antisolvent effect of SC CO<sub>2</sub> plays a key role to obtain PE-b-PEO nanocrystals on GO.

**Further Decoration of GO Sheets with Au NPs and CdTe NPs by PE-b-PEO as Interlinker.** Because of the amphiphilic property of the block copolymer PE-b-PEO decorated on GO, this nanohybrid could open a new route to introduce potential use in many fields such as nanocomposites. Furthermore, the

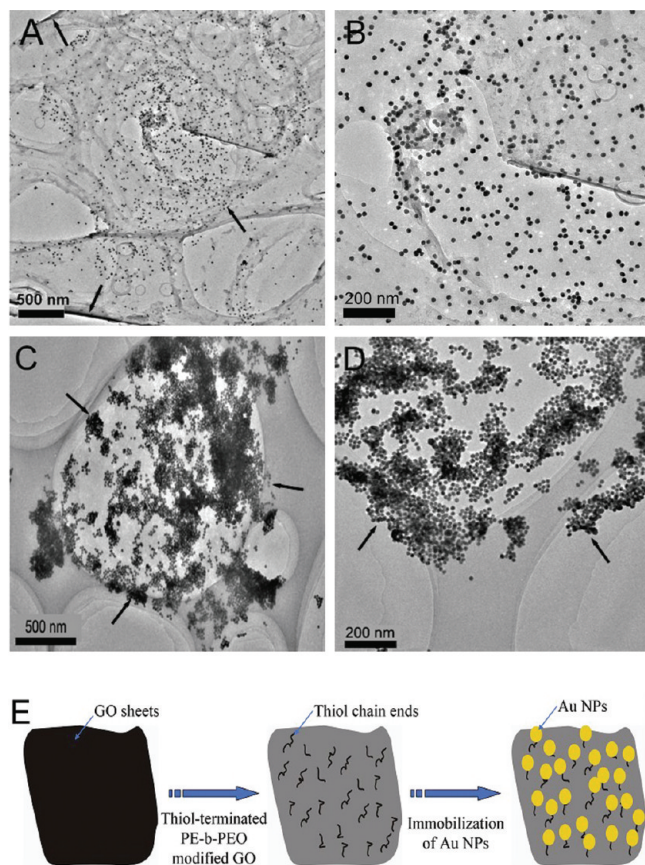


**Figure 7.** TEM images of the Au NPs-decorated thiol-terminated PE-b-PEO/GO hybrid prepared with two assemble methods: (A, B) incubation method; (C, D) mixed method. The edge of GO sheets with Au NPs has been marked by the black arrows. (E) Schematic representation of the procedure for immobilization of Au NPs on thiol-terminated PE-b-PEO/GO nanohybrid.

obtained nanohybrid structure can be used as the template to fabricate hybrid, multifunctional structures. As a proof-of-concept, we immobilized the as-prepared Au NPs and CdTe NPs on the PE-b-PEO/GO nanohybrids.

Due to the PEO domains contain large amount of  $-OH$  group which can be modified with various functional groups, so that multifunctional structure on the basis of the PE-b-PEO/GO nanohybrid can be achieved. In this work, we immobilized Au NPs on the thiol-terminated PE-b-PEO/GO nanohybrid. Foremost, we synthesized thiol-terminated PE-b-PEO and citrate-capped Au NPs. The FTIR spectrum of thiol-terminated PE-b-PEO and the UV-vis adsorption spectrum of Au NPs are shown in the SI (Figures S2 and S3), respectively. Following the same experimental procedure with DMSO as the solvent, GO sheets were modified by the block copolymer with thiol groups present in the PEO domains. Two assemble methods introduced in the Experimental Section were used to immobilize the as-prepared Au NPs on the thiol-terminated PE-b-PEO/GO nanohybrid. The typical TEM images of Au NPs-decorated block copolymer/GO hybrid were displayed in Figure 7. We find that the patterning Au NPs area density could be easily controlled by the assemble methods. From the overlook images (Figure 7A,C), it is observed that the well circumscribed Au NPs are distributed uniformly on the surface of GO, which clearly indicates that the NPs have been successfully loaded on the thiol-terminated PE-b-PEO/GO

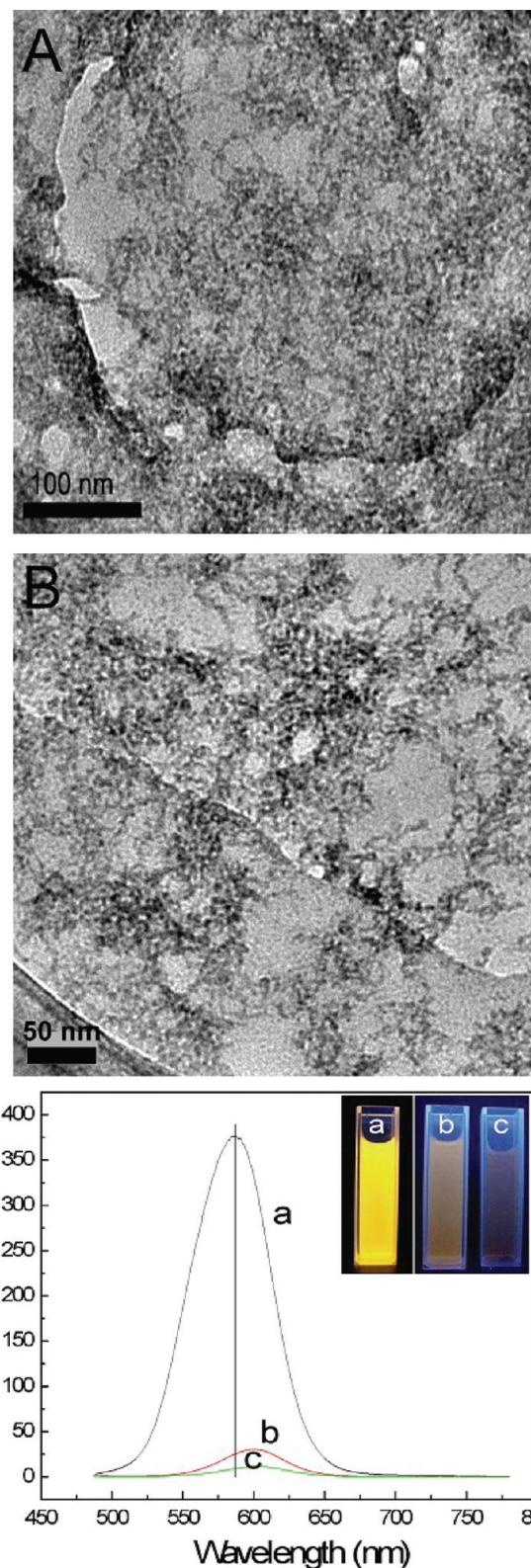


**Figure 8.** (A) and (B) TEM images of CdTe NPs immobilization on PE-b-PEO/GO nanohybrid. (C) Photoluminescence (PL) spectra of (a) CdTe NPs, (b) GO-CdTe, and (c) PE-b-PEO/GO-CdTe samples. The excitation wavelength is 468 nm. The inset of (C) shows photographs of the emission colors of the corresponding samples under the radiation of a UV lamp. The CdTe NPs sample (a) was added with the same amount of pure DMSO as (b) and (c).

nanohybrid. The sizes of Au NPs ranging from 15 to 20 nm are shown in Figure 7B,D. The TEM images show that the method of immobilizing Au NPs by robust Au—S bonds can effectively produce homogeneous and high-loading Au NPs on the surface of GO. The schematic representation of the procedure for immobilization of Au NPs on thiol-terminated PE-b-PEO/GO nanohybrid is shown in Figure 7E. This Au NPs/GO hybrid is of great interest in various areas of catalysis, sensors, and nanobiotechnology.<sup>13,61,84</sup>

Furthermore, the PE-b-PEO/GO nanohybrid was also decorated with semiconductor CdTe NPs in this work due to its potential application in the fields of biolabeling/bioimaging, solar cells, and optoelectronic devices.<sup>85–87</sup> Some attempts have been made to synthesize carbon nanotubes or GO-based CdTe nanohybrids, which can extend the applications and reinforce the pristine properties of simplex CdTe and carbon materials.<sup>88–90</sup> The assembly of semiconducting quantum dots (QDs) onto CNTs or graphene can result in the significant fluorescence quenching of the semiconducting QD due to the energy/electron transfer between the carbon materials and QDs, which is the critical property for novel applications in photovoltaic devices.<sup>91–93</sup> Figure 8A,B shows TEM images of the CdTe NPs-decorated PE-b-PEO/GO hybrid. It can be clearly seen that the GO sheets are well decorated with uniform CdTe NPs by PE-b-PEO interlinking. As a comparison, the GO sheets without coated block copolymer were also employed to examine attachment of the CdTe NPs under the same conditions. However, CdTe NPs aggregate together severely on the GO sheets (Figure S4 of the SI). It indicates that the block copolymer PE-b-PEO can efficiently immobilize CdTe NPs besides modifying the GO sheets. Figure 8C illustrates the PL spectra of CdTe NPs and PE-b-PEO/GO-CdTe samples. The PL spectrum of the mixed sample of GO and CdTe NPs is also shown for comparison. Upon light excitation at 468 nm, the CdTe NPs mixed with pure DMSO exhibit luminescence with a strong emission at 587 nm (trace a, Figure 8C). Its emission is largely quenched after mixing with GO (trace b, Figure 8C) and further quenched after the formation of PE-b-PEO/GO-CdTe hybrids (trace c, Figure 8C). The photographs of the emission colors of the corresponding samples under the radiation of a UV lamp are shown in the inset of Figure 8C. The color variation of the samples is another evidence that the fluorescence quenching of CdTe NPs is strongly affected by their interactions with GO sheets as well as PE-b-PEO interlinker. The drastic decrease in the fluorescence intensity of CdTe NPs upon mixing with GO sheets indicates that the nonirradiative decay path occurs as a result of electron transfer from CdTe NPs to GO sheets. The quenching becomes more notable for PE-b-PEO/GO-CdTe hybrids, indicating that the modification of PE-b-PEO on GO enhances the nonradiative decay processes due to the increased electron transfer from CdTe NPs to GO sheets. The PL spectra of the systems provide further evidence for the successful decoration of CdTe NPs onto GO sheets through PE-b-PEO interlinking.

## CONCLUSIONS

We present a facile and efficient approach to modify an amphiphilic double-crystalline block copolymer PE-b-PEO on the surface of GO sheets with the assistance of SC CO<sub>2</sub>. Varying decorated patterns of PE-b-PEO on GO were obtained in different solvent systems and at different SC CO<sub>2</sub> pressures. On the basis of the analysis of the results from FTIR and Raman

spectra, it revealed that there exist significant interactions between block copolymer chains and GO sheets. We found that the solvent system and the SC CO<sub>2</sub> have significant influence on the crystallization, aggregation, or assembly behaviors of PE-b-PEO molecular chains on the GO sheets. The formation mechanism of the distinct nanohybrid structures is attributed to a relevant easy heteronucleation and the limited crystal growth of the block polymer on the surface of GO. The resulting PE-b-PEO/GO nanohybrids can be promisingly applied not only in producing graphene-based nanocomposites, but also in acting as a template to fabricate hybrid, multifunctional structures due to the unique properties of PE-b-PEO. As an example, Au NPs and CdTe NPs were well-immobilized on the GO sheets using PE-b-PEO as the interlinker. With the thiol-terminated PE-b-PEO as an interlinker, Au NPs can be densely assembled on the surface of GO via robust Au—S bonds. And we found that the patterning Au NP's area density could be easily controlled by the assembly methods. Furthermore, the photoluminescence quenching of CdTe NPs was more notable for the PE-b-PEO/GO-CdTe hybrid compared to the GO-CdTe hybrid, suggesting that the electron transfer from the CdTe NPs to the GO sheets was enhanced by using the PE-b-PEO interlinker. These hybrid multifunctional structures are of great interest in various areas such as catalysis, nanobiotechnology, and photovoltaic devices.

## ASSOCIATED CONTENT

**S Supporting Information.** Detailed procedures for fabrication of thiol-terminated PE-b-PEO, Au NPs and CdTe NPs, FTIR spectrum of thiol-terminated PE-b-PEO, UV-vis adsorption spectrum of Au NPs, and TEM images of PE-b-PEO/GO nanohybrid produced without the treatment of SC CO<sub>2</sub> and CdTe NPs attachment on the pure GO sheets. This material is available free of charge via the Internet at <http://pubs.acs.org>.

## AUTHOR INFORMATION

### Corresponding Author

\*Tel.: +86 371 67767827; Fax: +86 371 67767827; E-mail: qunxu@zzu.edu.cn.

## ACKNOWLEDGMENT

We are grateful for the National Natural Science Foundation of China (Grant Nos. 20974102, 50955010), the financial support from the Program for New Century Excellent Talents in Universities (NCET).

## REFERENCES

- (1) Lee, C.; Wei, X.; Kysar, J. W.; Hone, J. *Science* **2008**, *321*, 385–388.
- (2) Bolotin, K. I.; Sikes, K. J.; Jiang, Z.; Kilma, M.; Fudenberg, G.; Hone, J.; Kim, P.; Stormer, H. L. *Solid State Commun.* **2008**, *146*, 351–355.
- (3) Balandin, A. A.; Ghosh, S.; Bao, W.; Calizo, I.; Teweldebrhan, D.; Miao, F.; Lau, C. N. *Nano Lett.* **2008**, *8*, 902–907.
- (4) Ruoff, R. *Nat. Nanotechnol.* **2008**, *3*, 10–11.
- (5) He, H. K.; Gao, C. *Chem. Mater.* **2010**, *22*, 5054–5064.
- (6) Dreyer, D. R.; Park, S.; Bielawski, C. W.; Ruoff, R. S. *Chem. Soc. Rev.* **2010**, *39*, 228–240.
- (7) Robinson, J. T.; Perkins, F. K.; Snow, E. S.; Wei, Z. Q.; Sheehan, P. E. *Nano Lett.* **2008**, *8*, 3137–3140.
- (8) Liu, Y.; Yu, D. S.; Zeng, C.; Miao, Z. C.; Dai, L. M. *Langmuir* **2010**, *26*, 6158–6160.

- (9) Zhang, J. L.; Zhang, F.; Yang, H. J.; Huang, X. L.; Liu, H.; Zhang, J. Y.; Guo, S. W. *Langmuir* **2010**, *26*, 6083–6085.
- (10) Xu, J. J.; Wang, K.; Zu, S. Z.; Han, B. H.; Wei, Z. X. *ACS Nano* **2010**, *4*, 5019–5026.
- (11) Yang, X. M.; Tu, Y. F.; Li, L.; Shang, S. M.; Tao, X. M. *ACS Appl. Mater. Interfaces* **2010**, *2*, 1707–1713.
- (12) Huang, Y. J.; Qin, Y. W.; Zhou, Y.; Niu, H.; Yu, Z. Z.; Dong, J. Y. *Chem. Mater.* **2010**, *22*, 4096–4102.
- (13) Goncalves, G.; Marques, P. A. A. P.; Granadeiro, C. M.; Nogueira, H. I. S.; Singh, M. K.; Gracio, J. *Chem. Mater.* **2009**, *21*, 4796–4802.
- (14) Williams, G.; Kamat, P. V. *Langmuir* **2009**, *25*, 13869–13873.
- (15) Chen, S.; Zhu, J. W.; Wu, X. D.; Han, Q. F.; Wang, X. *ACS Nano* **2010**, *4*, 2822–2830.
- (16) Shen, J. F.; Hu, Y. Z.; Shi, M.; Li, N.; Ma, H. W.; Ye, M. X. *J. Phys. Chem. C* **2010**, *114*, 1498–1503.
- (17) He, H. K.; Gao, C. *ACS Appl. Mater. Interfaces* **2010**, *2*, 3201–3210.
- (18) Kamat, P. V. *J. Phys. Chem. Lett.* **2010**, *1*, 520–527.
- (19) Ramanathan, T.; Abdala, A. A.; Stankovich, S.; Dikin, D. A.; Herrera-Alonso, M.; Piner, R. D.; Adamson, D. H.; Schniepp, H. C.; Chen, X.; Ruoff, R. S.; Nguyen, S. T.; Aksay, I. A.; Prud'homme, R. K.; Brinson, L. C. *Nat. Nanotechnol.* **2008**, *3*, 327–331.
- (20) Stankovich, S.; Piner, R. D.; Chen, X.; Wu, N.; Nguyen, S. T.; Ruoff, R. S. *J. Mater. Chem.* **2006**, *16*, 155–158.
- (21) Niyogi, S.; Bekyarova, E.; Itkis, M. E.; McWilliams, J. L.; Hamon, M. A.; Haddon, R. C. *J. Am. Chem. Soc.* **2006**, *128*, 7720–7721.
- (22) Stankovich, S.; Piner, R.; Nguyen, S. T.; Ruoff, R. S. *Carbon* **2006**, *44*, 3342–3347.
- (23) Lomeda, J. R.; Doyle, C. D.; Kosynkin, D. V.; Hwang, W. F.; Tour, J. M. *J. Am. Chem. Soc.* **2008**, *130*, 16201–16206.
- (24) Liu, Z.; Robinson, J. T.; Sun, X.; Dai, H. J. *J. Am. Chem. Soc.* **2008**, *130*, 10876–10877.
- (25) Wu, J. H.; Tang, Q. W.; Sun, H.; Lin, J. M.; Ao, H. Y.; Huang, M. L.; Huang, Y. F. *Langmuir* **2008**, *24*, 4800–4805.
- (26) Shan, C.; Yang, H.; Han, D.; Zhang, Q.; Ivaska, A.; Niu, L. *Langmuir* **2009**, *25*, 12030–12033.
- (27) Bai, H.; Xu, Y.; Zhao, L.; Li, C.; Shi, G. *Chem. Commun.* **2009**, 1667–1669.
- (28) Salavagione, H. J.; Gomez, M. A.; Martinez, G. *Macromolecules* **2009**, *42*, 6331–6334.
- (29) Li, G. L.; Liu, G.; Li, M.; Wan, D.; Neoh, K. G.; Kang, E. T. *J. Phys. Chem. C* **2010**, *114*, 12742–12748.
- (30) Szleifer, I.; Yerushalmi-Rozen, R. *Polymer* **2005**, *46*, 7803–7818.
- (31) Wang, Z. M.; Liu, Q. C.; Zhu, H.; Liu, H. F.; Chen, Y. M.; Yang, M. S. *Carbon* **2007**, *45*, 285–292.
- (32) Nativ-Roth, E.; Shvartzman-Cohen, R.; Bounioux, C.; Florent, M.; Zhang, D. S.; Szleifer, I.; Yerushalmi-Rozen, R. *Macromolecules* **2007**, *40*, 3676–3685.
- (33) Wang, W. R.; Xie, X. M.; Ye, X. Y. *Carbon* **2010**, *48*, 1680–1683.
- (34) Chan, S. C.; Kuo, S. W.; Lu, C. H.; Lee, H. F.; Chang, F. C. *Polymer* **2007**, *48*, 5059–5068.
- (35) Jenekhe, S. A.; Chen, X. L. *Science* **1998**, *279*, 1903–1907.
- (36) Jain, S.; Bates, F. S. *Science* **2003**, *300*, 460–464.
- (37) Raez, J.; Manners, I.; Winnik, M. A. *J. Am. Chem. Soc.* **2002**, *124*, 10381–10395.
- (38) Chouchair, A.; Eisenberg, A. *Eur. Phys. J. E* **2003**, *10*, 37–44.
- (39) Chen, E.; Xia, Y.; Graham, M. J.; Foster, M. D.; Mi, Y.; Wu, W.; Cheng, S. Z. D. *Chem. Mater.* **2003**, *15*, 2129–2135.
- (40) Bhargava, P.; Zheng, J. X.; Li, P.; Quirk, R.; Harris, F. W.; Cheng, S. Z. D. *Macromolecules* **2006**, *39*, 4880–4888.
- (41) Massey, J.; Power, K. N.; Manners, I.; Winnik, M. A. *J. Am. Chem. Soc.* **1998**, *120*, 9533–9540.
- (42) Kataoka, K.; Harada, A.; Nagasaki, Y. *Adv. Drug Delivery Rev.* **2001**, *47*, 113–131.
- (43) Savic, R.; Luo, L. B.; Eisenberg, A. *Science* **2003**, *300*, 615–618.
- (44) Kim, B. H.; Kim, J. Y.; Jeong, S. J.; Hwang, J. O.; Lee, D. H.; Shin, D. O.; Choi, S. Y.; Kim, S. O. *ACS Nano* **2010**, *4*, 5464–5470.
- (45) Zhang, Z. W.; Xu, Q.; Chen, Z. M.; Yue, J. *Macromolecules* **2008**, *41*, 2868–2873.
- (46) Fujiwara, T.; Miyamoto, M.; Kimura, Y.; Iwata, T.; Doi, Y. *Macromolecules* **2001**, *34*, 4043–4050.
- (47) Ho, R. M.; Hsieh, P. Y.; Tseng, W. H.; Lin, C. C.; Huang, B. H.; Lotz, B. *Macromolecules* **2003**, *36*, 9085–9092.
- (48) Nojima, S.; Akutsu, Y.; Akaba, M.; Tanimoto, S. *Polymer* **2005**, *46*, 4060–4067.
- (49) Takeshita, H.; Fukumoto, K.; Ohnishi, T.; Ohkubo, T.; Miya, M.; Takenaka, K.; Shiomi, T. *Polymer* **2006**, *47*, 8210–8218.
- (50) Nojima, S.; Kiji, T.; Ohguma, Y. *Macromolecules* **2007**, *40*, 7566–7572.
- (51) Li, T.; Wang, W. J.; Liu, R.; Liang, W. H.; Zhao, G. F.; Li, Z. Y.; Wu, Q.; Zhu, F. M. *Macromolecules* **2009**, *42*, 3804–3810.
- (52) Sun, L.; Liu, Y. X.; Zhu, L.; Hsiao, B. S.; Avila-Orta, C. A. *Polymer* **2004**, *45*, 8181–8193.
- (53) Castillo, R. V.; Arnal, M. L.; Muller, A. J.; Hamley, I. W.; Castelletto, V.; Schmalz, H.; Abetz, V. *Macromolecules* **2008**, *41*, 879–889.
- (54) Cao, W. Y.; Tashiro, K.; Hanesaka, M.; Takeda, S.; Masunaga, H.; Sasaki, S.; Takata, M. *J. Phys. Chem. B* **2009**, *113*, 2338–2346.
- (55) Araújo, E. S.; Rieumont, J.; Nogueiras, C.; de Oliveira, H. P. *Eur. Polym. J.* **2010**, *46*, 1854–1859.
- (56) Unsworth, L. D.; Sheardown, H.; Brash, J. L. *Langmuir* **2005**, *21*, 1036–1041.
- (57) Lin, Y.; Allard, L. F.; Sun, Y. P. *J. Phys. Chem. B* **2004**, *108*, 3760–3764.
- (58) Li, B.; Li, L. Y.; Wang, B. B.; Li, C. Y. *Nat. Nanotechnol.* **2009**, *4*, 358–362.
- (59) Hummers, W. S.; Offerman, R. E. *J. Am. Chem. Soc.* **1958**, *80*, 1339.
- (60) Kovtyukhova, N. I.; Ollivier, P. J.; Martin, B. R.; Mallouk, T. E.; Chizhik, S. A.; Buzaneva, E. V.; Gorchinskiy, A. D. *Chem. Mater.* **1999**, *11*, 771–778.
- (61) Fang, Y. X.; Guo, S. J.; Zhu, C. Z.; Zhai, Y. M.; Wang, E. *Langmuir* **2010**, *26*, 11277–11282.
- (62) Zhang, H.; Zhou, Z.; Yang, B.; Gao, M. Y. *J. Phys. Chem. B* **2003**, *107*, 8–13.
- (63) Hamley, I. W. *Block Copolymers in Solution Fundamentals and Applications*; Wiley: New York, 2005.
- (64) He, M. J.; Chen, W. X.; Dong, X. X. *Polymer Physics*; Fudan University Press: Shanghai (China), 2000; Chapter 3.
- (65) Zhang, F.; Zhang, H.; Zhang, Z. W.; Chen, Z. M.; Xu, Q. *Macromolecules* **2008**, *41*, 4519–4523.
- (66) Eskilsson, K.; Tiberg, F. *Macromolecules* **1998**, *31*, 5075–5083.
- (67) Grant, L. M.; Tiberg, F.; Ducker, W. A. *J. Phys. Chem. B* **1998**, *102*, 4288–4294.
- (68) Connell, S. D.; Collins, S.; Fundin, J.; Yang, Z.; Hamley, I. W. *Langmuir* **2003**, *19*, 10449–10453.
- (69) Trijillo, M.; Arnal, M. L.; Muller, A. J.; Bredeau, S.; Bonduel, D.; Dubois, Ph.; Hamley, I. W.; Castelletto, V. *Macromolecules* **2008**, *41*, 2087–2095.
- (70) Huang, X. D.; Goh, S. H. *Macromolecules* **2001**, *34*, 3302–3307.
- (71) Wakeland, S.; Martinez, R.; Grey, J. K.; Luhrs, C. C. *Carbon* **2010**, *48*, 3463–3470.
- (72) Zhang, Y. L.; Guo, Li.; Wei, S.; He, Y. Y.; Xia, H.; Chen, Q. D.; Sun, H. B.; Xiao, F. S. *Nano Today* **2010**, *5*, 15–20.
- (73) Liu, J. C.; Wang, Y. J.; Xu, S. P.; Sun, D. D. *Mater. Lett.* **2010**, *64*, 2236–2239.
- (74) Webber, G. B.; Wanless, E. J.; Butun, V.; Armes, S. P.; Biggs, S. *Nano Lett.* **2002**, *2*, 1307–1313.
- (75) Bower, D. I.; Maddams, W. F. *the Vibrational Spectroscopy of Polymers*; Cambridge University Press: Cambridge (UK), 1989.
- (76) Zheng, X. L.; Xu, Q. *J. Phys. Chem. B* **2010**, *114*, 9435–9444.
- (77) Baskaran, D.; Mays, J. W.; Bratcher, M. S. *Chem. Mater.* **2005**, *17*, 3389–3397.
- (78) Shen, Z. Q.; Simon, G. P.; Cheng, Y. B. *Polymer* **2002**, *43*, 4251–4260.
- (79) Rao, A. M.; Eklund, P. C.; Bandow, S.; Thess, A.; Smalley, R. E. *Nature* **1997**, *388*, 257–259.

- (80) Voggu, R.; Rout, C. S.; Franklin, A. D.; Fisher, T. S.; Rao, C. N. R. *J. Phys. Chem. C* **2008**, *112*, 13053–13056.
- (81) Chatterjee, T.; Yurekli, K.; Hadjiev, V. G.; Krishnamoorti, R. *Adv. Funct. Mater.* **2005**, *15*, 1832–1838.
- (82) Shvartzman-Cohen, R.; Monje, I.; Florent, M.; Frydman, V.; Goldfarb, D.; Yerushalmi-Rozen, R. *Macromolecules* **2010**, *43*, 606–614.
- (83) Span, R.; Wagner, W. *J. Phys. Chem. Ref.* **1996**, *25*, 1509.
- (84) Shen, C. M.; Hui, C.; Yang, T. Z.; Xiao, C. W.; Tian, J. F.; Bao, L. H.; Chen, S. T.; Ding, H.; Gao, H. *J. Chem. Mater.* **2008**, *20*, 6939–6944.
- (85) Sun, J.; Wang, L. W.; Buhro, W. E. *J. Am. Chem. Soc.* **2008**, *130*, 7997–8005.
- (86) Cho, W.; Kim, H. S.; Kim, Y. J.; Jang, S. Y.; Park, J.; Kim, J. G.; Kim, Y. J.; Cha, E. H. *Chem. Mater.* **2008**, *20*, 5600–5609.
- (87) Zhang, Z. L.; Tang, Z. Y.; Kotov, N. A.; Glotzer, C. *Nano Lett.* **2007**, *7*, 1670–1675.
- (88) Guldi, D. M.; Rahman, G. M. A.; Sgobba, V.; Kotov, N. A.; Bonifazi, D.; Prato, M. *J. Am. Chem. Soc.* **2006**, *128*, 2315–2323.
- (89) Jia, N. Q.; Lian, Q.; Shen, H. B.; Wang, C.; Li, X. Y.; Yang, Z. N. *Nano Lett.* **2007**, *7*, 2976–2980.
- (90) Wang, Y.; Lu, J.; Tang, L. H.; Chang, H. X.; Li, J. H. *Anal. Chem.* **2009**, *81*, 9710–9715.
- (91) Li, Q. W.; Sun, B. Q.; Kinloch, I. A.; Zhi, D.; Sirringhaus, H.; Windle, A. H. *Chem. Mater.* **2006**, *18*, 164–168.
- (92) Feng, M.; Sun, R. Q.; Zhan, H. B.; Chen, Y. *Carbon* **2010**, *48*, 1177–1185.
- (93) Chen, Z. Y.; Berciaud, S.; Nuckolls, C.; Heinz, T. F.; Brus, L. E. *ACS Nano* **2010**, *4*, 2964–2968.